

VLAD-Grasp: Zero-shot Grasp Detection via Vision-Language Models

Manav Kulshrestha¹, S. Talha Bukhari¹, Damon Conover², Aniket Bera¹

Abstract— Robotic grasping is a fundamental capability for autonomous manipulation; however, most existing methods rely on large-scale expert annotations and necessitate retraining to handle new objects. We present VLAD-Grasp, a Vision-Language model Assisted zero-shot approach for Detecting grasps. From a single RGB-D image, our method (1) prompts a large vision-language model to generate a goal image where a straight rod “impales” the object, representing an antipodal grasp, (2) predicts depth and segmentation to lift this generated image into 3D, and (3) aligns generated and observed object point clouds via principal component analysis and correspondence-free optimization to recover an executable grasp pose. Unlike prior work, our approach is training-free and does not rely on curated grasp datasets. Despite this, VLAD-Grasp achieves performance that is competitive with or superior to that of state-of-the-art supervised models on the Cornell and Jacquard datasets. We further demonstrate zero-shot generalization to novel real-world objects on a Franka Research 3 robot, highlighting vision-language foundation models as powerful priors for robotic manipulation. More available at: manavkulshrestha.github.io/vlad

I. INTRODUCTION

Grasp synthesis is the task of determining a stable gripper pose to pick an object. Reliable robotic grasping underlies a wide range of downstream tasks, such as rearrangement [1, 2], sorting [3], assembly [4], and human–robot collaboration [5, 6]. Hence, grasp synthesis is a fundamental capability required for autonomous operation in unstructured environments. The problem is difficult due to the diversity of object geometries, material properties, and task constraints. This difficulty is further amplified when robots must grasp objects that have never been encountered before. Therefore, common-sense reasoning capabilities are a necessary precursor to a robust grasp synthesis method.

Classical approaches to grasp detection rely on analytic models of contact mechanics and object geometry to predict grasp stability [7, 8]. These methods provide useful insights, but are limited by simplifying heuristics, which restrict their ability to generalize across arbitrary shapes and materials. Learning-based methods have since become dominant, enabled by large-scale grasp datasets [9]. Deep networks trained on annotated grasp rectangles [10] or physics-based labels [11] achieve high accuracy in distribution. However, their performance is upper-bounded by the coverage and quality of the training datasets. Collecting expert-labeled data is costly and time-intensive, and simulated grasps are

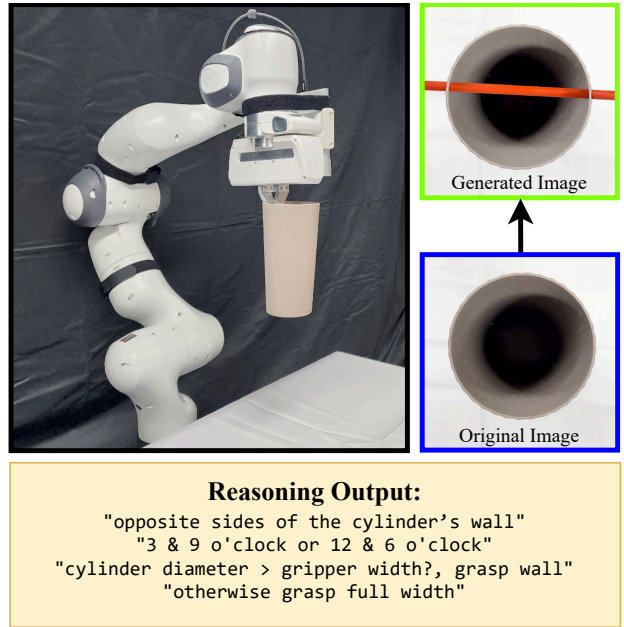


Fig. 1: VLAD captures an image of the target object and queries a VLM using the cropped view alongside sequential guiding prompt to reason about the object’s geometry and feasible grasps. The VLM then generates a goal image depicting a virtual rod “impaling” the object, which encodes the antipodal grasp axis. This axis is reconstructed in 3D and aligned with the observed scene to yield an executable grasp pose.

often biased toward restricted families of grasp modes [12]. As a result, even state-of-the-art supervised methods fail to generalize to novel categories, cluttered environments, and real-world deployment scenarios. Recent work has attempted to address this gap by incorporating semantic or multimodal cues into grasp prediction, for example, through language-conditioned grasping [13–15] or segmentation-guided detection [16]. While these approaches improve task relevance, they still depend on retraining with labeled grasp data and, therefore, inherit the same scalability limitations.

In this work, we ask a different question: Can the reasoning and generative capabilities of large vision–language models (VLMs), trained on internet-scale multimodal data, be directly exploited for robotic grasping *without any task-specific training or fine-tuning*? VLMs encode broad visual–semantic knowledge from massive image–text corpora, including implicit understanding of object affordances and human–object interactions [17–19]. This makes them a compelling prior for robotic grasping, where explicit supervision is costly and incomplete.

We introduce VLAD-Grasp, a zero-shot grasp synthesis framework that leverages pretrained VLMs to propose and

¹Manav Kulshrestha, S. Talha Bukhari, and Aniket Bera are with the IDEAS Lab, Department of Computer Science, Purdue University, West Lafayette, IN, USA. {mkulshre, bukhars, aniketbera}@purdue.edu

²Damon Conover is with the DEVCOM Army Research Laboratory, Adelphi, MD, USA. {damon.m.conover.civ@army.mil}

execute feasible grasps on unseen objects. Our approach operates on a single RGB-D observation of the scene. First, the robot queries a VLM with the object image and a sequence of guiding textual prompt to generate a goal image containing a virtual rod representing the antipodal grasp axis. Second, monocular depth prediction and segmentation lift the generated image into 3D. Third, we align the generated and real object point clouds via principal component analysis and correspondence-free point cloud optimization, yielding an executable grasp pose for the robot. Crucially, our approach does not require any expert grasp datasets, supervision, or fine-tuning.

The novelty of VLAD lies in combining three elements: (1) *Zero-shot grasp reasoning* via VLM prompts, which removes the need for curated grasp annotations; (2) *Geometric consistency alignment* between generated and observed data, which bridges the domain gap between synthetic goal images and physical scenes; and (3) *Scalable deployment* on real hardware, validating that foundation model priors can be directly transferred to physical grasping without retraining.

The contributions of this paper are:

- An end-to-end, zero-shot grasp synthesis pipeline which maps single RGB-D observations to executable robot grasps without additional training or expert supervision.
- A geometric alignment procedure that combines monocular depth prediction, PCA-based registration, and correspondence-free point cloud optimization to consistently recover grasp poses from generated images.
- Extensive evaluations on the Cornell and Jacquard datasets, showing comparable or superior performance (up to +30% success rate) relative to state-of-the-art supervised baselines.

II. RELATED WORK

A. Large Vision-Language Models

Pretrained large language models [20, 21] have brought about a paradigm shift in modern deep learning. Here, the goal is to scale compute and data to achieve higher performance as well as emergent behaviors and reasoning capabilities. However, as models continue to scale, their capabilities are limited by a finite supply of high-quality text data and the inherent limitations of single-modality architectures [22]. Capturing and processing information from the real world involves reasoning about the complex relationships across different modalities [23], which motivates the development of Vision-Language Models (VLMs): Architectures that process visual (images and video) and textual information together to provide more comprehensive reasoning capabilities. State-of-the-art VLMs include CLIP [24], BLIP [25], Flamingo [26], GPT-4V [27], and Gemini [28]. In this work, we leverage the cross-modality reasoning capabilities of VLMs to perform zero-shot grasp detection.

B. Large-Scale Pretraining for Robotics

Traditional data-driven methods in robotics have been trained on task-specific datasets, which are challenging to

curate exhaustively for the task at hand, and the trained methods fail to generalize beyond the experimental setting. Recent years have seen a push for large-scale data collection and pre-training to solve robotics tasks [29, 30], inspired by the success of large language models from training on web-scale datasets. The emergent behaviors from large-scale pretraining include common-sense reasoning across various modalities, such as text, images, audio, and video. Kapelyukh et al. [31] demonstrate human-like object rearrangement skills using diffusion models trained on web-scale data. Shridhar et al. [13] utilize CLIP for semantic reasoning and Transporter & Perceiver for spatial reasoning. Karamcheti et al. [32] presents a framework for language-driven representation learning in robotics by capturing semantic, spatial, and temporal representations learned from videos and captions. Unlike previous work, we propose an approach that leverages the visual and textual reasoning capabilities of large vision-language models to infer grasping from 2D images alone, without requiring explicit training on expert data.

C. Grasp Detection

Detecting grasp candidates is a core task in robotic manipulation. Classical methods used geometric approaches to generate and evaluate stable grasps [7–9]. With the advent of modern deep learning, a wide range of approaches for grasp generation have been developed. Morrison et al. [33], Kumra et al. [34], Ainetter and Fraundorfer [35] train convolutional neural networks to detect grasps from RGB-D images. Mahler et al. [36], Mousavian et al. [37], Bukhari et al. [38] infer stable grasp distributions in 3D by ingesting object point clouds. Shridhar et al. [13], Xu et al. [14], Vuong et al. [15] leverage language information to guide grasp synthesis via text prompts. Noh et al. [16] incorporate large-scale pretraining of the Segment-Anything Model (SAM) to guide grasp detection via object masks.

However, all the aforementioned methods involve training on expert grasp data, which is time-consuming to collect and tedious to train reliably on [10, 39, 40]. Furthermore, such datasets may sometimes miss crucial intuitive grasp candidates that the employed expert was unable to model [12]. This upper bounds the performance of trained grasp detection methods, without incorporating intuitive reasoning. Instead, we propose using the reasoning capabilities of large language models to generate grasp candidates for images, without requiring any training on expert data (i.e., zero-shot).

III. METHODOLOGY

We tackle the problem of generating a grasp from a single RGB-D image of an object in a zero-shot manner, by leveraging large-scale VLMs. Our end-to-end approach for generating a grasp in image space is detailed in Fig. 2.

To reason about and utilize a large-scale multimodal generative model, which has been trained on the web and can process and generate both text and images in a unified manner. This model, given an image of the scene I_S containing the object o_S to grasp and a text query encoding the

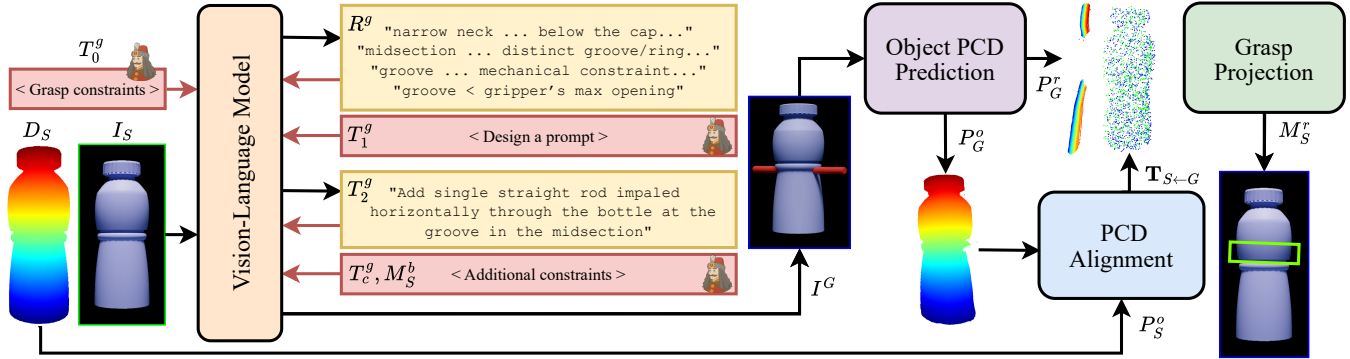


Fig. 2: Overview of our approach. We capture an RGB-D image (I_S, D_S) of the object and mask out background distractors. The RGB image I_S is provided to the VLM, following structured guiding prompts T_i^g , to help it reason R^g about object geometry and eventually produce a generated image I_G , where the goal grasp is indicated by a rod passing through the antipodal grasp points on the object’s surface. Following this, predict a point cloud P_G^o for the object in the generated image I_G and match it with the point cloud P_S^o for the object in the original image I_S

grasp constraints, can output an image I_G representing the goal grasp. In particular, the generated image I_G shows the grasp indicated by a rod r_G physically passing through the object o_G .

Next, we obtain a monocular depth estimate D_G for the generated image in addition to extracting segmentation masks for both the object M_G^o and the rod M_G^r . All of these are used to lift the generated image I_G into Cartesian space $\mathcal{C}_G \subseteq \mathbb{R}^3$ by generating a point cloud $P_G \subseteq \mathcal{C}_G$ and for the generated scene image I_G and associated point cloud subsets P_G^o, P_G^r for the object and the rod, respectively. Similarly, we also extract a segmentation mask M_S^o for the object o_S in the original scene I_S and use the measured depth D_S to generate a point cloud $P_S^o \subseteq \mathcal{C}_S \subseteq \mathbb{R}^3$ for it. Following this, we perform principal components-based pointcloud alignment, followed by correspondence-free optimization between the object pointclouds P_S^o (from the original scene) and P_G^o (from the generated image) to obtain an alignment transform $T_{S \leftarrow G}$. Lastly, we apply this transform to the rod point cloud P_G^r and project it down to the original image space S to obtain the rod mask M_S^r . Finally, we use this rod mask to calculate feasible grasp poses for the object in the original scene o_S .

A. Grasp Image Generation

Current state-of-the-art VLMs autoregressively learn an implicit joint linguistic–visual distribution $p_\theta(\mathcal{T}, \mathcal{I})$. This can later be conditioned on a sequence of elements $(x_k)_{k=1}^{t-1} \subseteq (\mathcal{T} \cup \mathcal{I})^{t-1}$ belonging to either modality, to generate $p_\theta(x_t | x_{t-1}, \dots)$ where $x_t \in \mathcal{T} \cup \mathcal{I}$ can also be from either modality. In our method, we aim to leverage the stronger reasoning capabilities of text-based language models while simultaneously incorporating image outputs to provide a more natural medium for representing geometric information and guiding the downstream grasping task.

To achieve this, we utilize a three-step prompting structure. First, we provide the model with an image I_S of the object from the initial scene and query it with a text prompt T_0^g which contains the constraints (gripper size and configuration, visibility in image space, etc.) for the desired grasp.

In order to minimize distractions for the model, we mask-out the background using a mask M_S^o of the object obtained using a state-of-the-art segmentation model. Following the model’s reasoning and reconciliation $p_\theta(R^g | I_S, T_0^g)$ of the grasp constraints with the object geometry, we further query it with a text prompt T_1^g to generate text which will be used directly as a prompt for the next step. In particular, we indicate that the model should utilize its previous reasoning R^g to generate a prompt T_2^g which, when queried with the original image I_S , should result in an image I_G showing a rod r_G being ‘impaled’ through the object o_G present.

This formulation of the grasp as a rod has three main advantages. First, representing the grasp as a physical object in the generated image helps ground the generation from the model in concepts within its training domain, rather than abstract concepts such as stability and affordances. Secondly, a straight rod implicitly encodes that the two grasp points are antipodal with respect to the object surface, which is suitable for our experimental setup, given the 2-finger gripper configuration. Third, a minimal object, such as a rod, prevents the focus bandwidth from shifting from the task at hand, ensuring better prompt adherence. We also augment the generated prompt T_2^g with additional constraints in the form of both text instructions T_c^g and an inpainting mask M_S^b (in practice, this is a background mask obtained by inverting the object mask M_S^o), to penalize modifications to the object o_G in the generated image I_G . Finally, we query the model with the constraint-augmented image generation prompt $p_\theta(I_G | T_c^g, T_2^g, M_S^b, I_S)$ to obtain a generated image I_G^o which represents the goal grasp.

B. Object Alignment

We explicitly include text prompts T_c^g and inpainting masks M_S^b to minimize changes to the object between the original image I_S and the generated image I_G . However, these specifications only add soft constraints for current state-of-the-art models for image editing. This allows us to provide conservative constraints in the text prompt T_c^g and directly use the background mask M_S^b without conflicting with the model’s logically consistent image generation capability in order to represent the full range of impaling rods (i.e.,

antipodal grasps). However, a consequence of this is that there are differences with respect to the specific objects represented in and the overall composition of the images I_S and I_G . The resulting difference in image spaces S and G makes it challenging to directly interpret the rod r_G in the generated image I_G as an actionable grasp pose for the object o_S in the original image I_S .

To address this, we align the object o_S in the original image with its counterpart o_G in the generated image, assuming spatial consistency within each image. For I_S , this consistency is inherent. At the same time, for I_G it is assumed to hold, given that modern large-scale vision-language models typically produce images with coherent spatial structure as a by-product of their large-scale training. As before, we obtain the masks M_G^o, M_G^r for both the object o_G and rod r_G in the generated image. Next, we utilize a state-of-the-art monocular depth estimation model to predict a depth estimate D_G for the generated image I_G and combine it with the masks to obtain estimated point clouds $P_G^o, P_G^r \subseteq \mathcal{C}_G \subseteq \mathbb{R}^3$ for each element o_G, r_G in the generated image. Note that we already have the object mask M_S^o and true depth D_S for the original image and, therefore, use it to also construct a point cloud $P_S^o \subseteq \mathcal{C}_S \subseteq \mathbb{R}^3$. Following this, we can perform object alignment for point clouds P_S^o, P_G^o in their respective Cartesian spaces $\mathcal{C}_S, \mathcal{C}_G$.

A key observation here is that while the object in the generated image may differ in pose and details, the overall shape for o_S and o_G remains largely consistent. Therefore, we can exploit this property to perform point cloud registration that is invariant to local features, but mindful of global shape. We mean-center both object point clouds P_S^o, P_G^o , estimate their covariance matrices, and perform eigen decompositions to obtain each of their respective top-3 components (i.e., eigenvectors $\mathbf{v}_i^{oS}, \mathbf{v}_i^{oG}$ associated with the largest three eigenvalues $\lambda_i^{oS}, \lambda_i^{oG}$). Following this, our optimal rotation becomes the following:

$$\mathbf{R}_{S \leftarrow G}^* = \arg \min_{\mathbf{R}^{i,j,k}} \mathcal{L}\{P_S^o, P_G^o | \mathbf{R}^{i,j,k}\}$$

where $(i, j, k) \in \{-1, 1\}^3$, \mathcal{L} is correspondence-free loss metric (we use Chamfer Distance [41]), and $\mathbf{R}^{i,j,k}$ is a candidate alignment rotation is given by:

$$\left[\mathbf{v}_1^{oS}, \mathbf{v}_2^{oS}, \mathbf{v}_3^{oS} \right] \left[i\mathbf{v}_1^{oG} \sqrt{\frac{\lambda_1^{oG}}{\lambda_1^{oS}}}, j\mathbf{v}_2^{oG} \sqrt{\frac{\lambda_2^{oG}}{\lambda_2^{oS}}}, k\mathbf{v}_3^{oG} \sqrt{\frac{\lambda_3^{oG}}{\lambda_3^{oS}}} \right]^{-1}$$

Putting this all together, the following optimal transform $\mathbf{T}_{S \leftarrow G}$ aligns P_G^o with P_S^o by minimizing $\mathcal{L}\{P_S^o, \mathbf{T}_{S \leftarrow G} P_G^o\}$:

$$\mathbf{T}_{S \leftarrow G} = \begin{bmatrix} \mathbf{I}_3 & \frac{1}{m} \mathbf{1}_m^\top P_S^o \\ \mathbf{0} & 1 \end{bmatrix} \begin{bmatrix} \mathbf{R}_{S \leftarrow G}^* & \mathbf{0} \\ \mathbf{0} & 1 \end{bmatrix} \begin{bmatrix} \mathbf{I}_3 & -\frac{1}{n} \mathbf{1}_n^\top P_G^o \\ \mathbf{0} & 1 \end{bmatrix}$$

where $\text{rows}(P_S^o) = m$ and $\text{rows}(P_G^o) = n$.

C. Grasp Projection

Following alignment, we obtain the ability to map elements from the generated cartesian space \mathcal{C}_G to the original cartesian space \mathcal{C}_S using the transformation $\mathbf{T}_{S \leftarrow G}$. Next, we can apply the transform to the rod pointcloud P_G^r to obtain its

image $P_S^r = \mathbf{T}_{S \leftarrow G}(P_G^r)^\top$ in the original Cartesian space. At this stage, the rod pointcloud P_S^r “impales” the object pointcloud P_S^o , indicating a 6-DoF grasp pose in the original Cartesian space \mathcal{C}_S . However, for our experimental setup, we project the rod point cloud P_S^r down to a rod mask M_S^r in the original image space S , for interpreting an oriented rectangle representation of the grasp, in line with [11].

For interpreting grasp rectangles from the rod mask M_S^r in the image space, we observe that any discontinuities in the rod r_G in the generated image I_G , and consequently, the rod mask M_S^r along its line of best fit must be a viable grasp location since it is where the rod passes through the object. Furthermore, the angle of the rod mask M_S^r can be used to obtain the gripper pose for the robot, given the camera extrinsics. The length of the discontinuity in the mask M_S^r would be a conservative estimate of the grasp width required to achieve force closure on the object. Note that there may be several discontinuities in the mask M_S^r resulting from the sparsity in the rod point cloud P_S^r , or the number of occlusions due to the object, only the latter of which should be interpreted as valid grasp locations. We sort these discontinuities by their run length, filter based on a viability threshold δ (in practice, a ratio of the object mask), and choose the optimal grasp location based on a selection heuristic that takes into account the overlap between the object M_S^o and rod mask M_S^r . Specifically, we obtain a rod discontinuity mask M_S^d (inverse of the rod mask M_S^r , but within the bounds of the rod r_S) and select locations that have IoU above some minimum threshold ϵ with the object mask M_S^o . Finally, we use all this information to generate a sequence of lower-level actions which, when executed, result in object o_S in the original scene being picked from the selection grasp point.

IV. EXPERIMENTS

For our approach, we employ the GPT-5 model [17] as the VLM in our method. Depth maps are generated by the ML Depth Pro model [42], and segmentations are generated by the Segment Anything Model (SAM) [43]. We evaluate our approach against state-of-the-art methods for grasp detection on images across the Cornell [11] (real) and Jacquard [10] (simulated) datasets. We use the following baseline methods for comparison: GR-ConvNet [34], GG-CNN [33], SE-ResUNet [35], GraspSAM [16], and LGD [15]. All baseline methods were trained on the datasets on an NVIDIA RTX 5080 GPU system, except LGD where we use the authors’ provided model checkpoint. Furthermore, we perform ablations to analyze the importance of the multi-step prompting structure, the effect of utilizing different VLMs, and the choice of cross-domain object point cloud alignment. Finally, we demonstrate our approach for robotic picking in the real world using a Frank Research 3 robot arm.

A. Zero-Shot Grasping

Following the experimental setup from prior work [40], we evaluate the performance of our approach zero-shot on unseen object classes from the Cornell (70) and Jacquard (97)

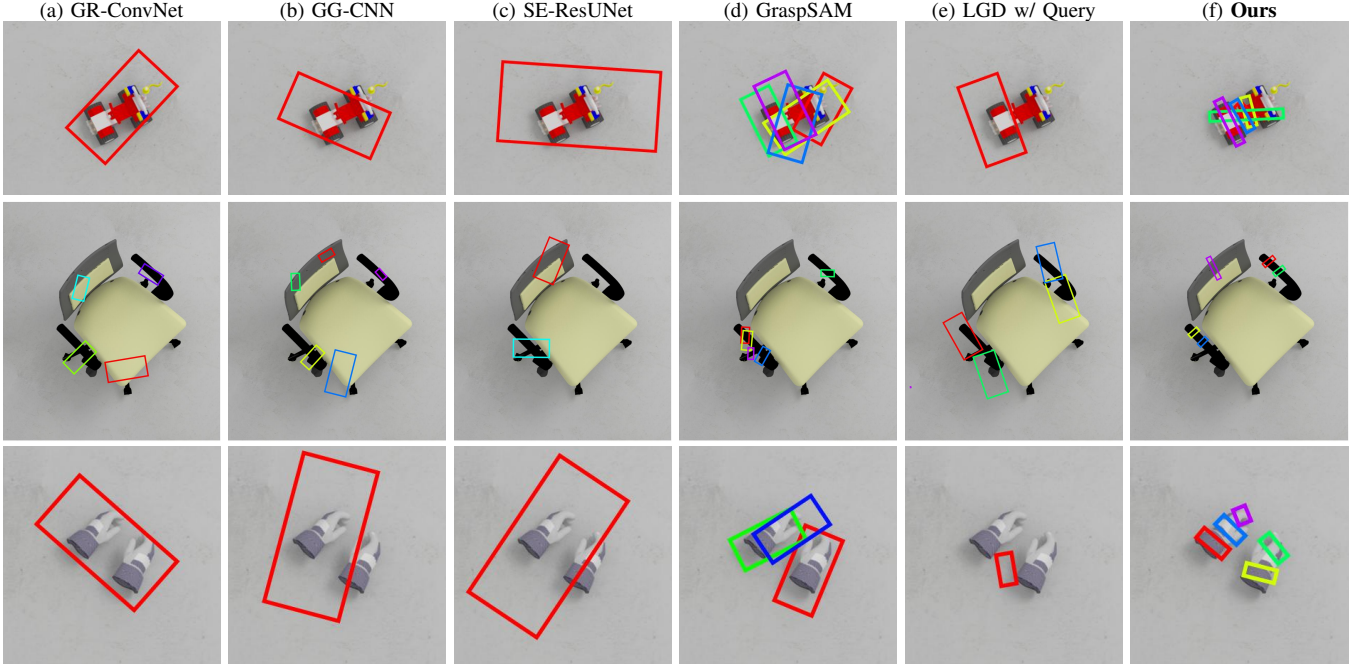


Fig. 3: Qualitative comparison of grasp detection on different objects. For each method, we show five grasps per object, although for some methods the grasp modalities may sometimes converge. Compared to baselines, our method detects more successful grasps across diverse object types. Prior methods often produce coarse or misaligned grasps, while our approach generates accurate and well-localized grasps that align with object geometry.

datasets. We note that the grasp annotations in the Jacquard dataset are not fully exhaustive. Therefore, a method that proposes grasps outside the dataset’s ground truth coverage will be unfairly penalized in the grasp success metrics (we discuss this in Sec. V-A). To account for this, we present results in Tab. I on a subset of the original unseen set, filtering out data points with fewer than 100 grasp annotations 100. For all baselines except LGD, we present results for the model trained on the seen subset and evaluated on the unseen subset of the same dataset. For LGD, we use the model pretrained on the GraspAnything++ dataset [15] and evaluate zero-shot on both datasets with and without language-guided queries, following a similar ablation from the original paper (which boasts competitive zero-shot transfer performance).

On the Cornell dataset, VLAD-Grasp achieves superior performance than all baselines, leading by $\sim 5\%$. In contrast, on the Jacquard dataset, our method achieves competitive results at second place, trailing by $\sim 3\%$. It is important to note that while our method operates zero-shot on both

datasets, all baselines apart from LGD have been directly trained on the datasets. All methods except SE-ResUNet and GraspSAM perform worse on the Jacquard dataset compared to the Cornell dataset, likely due to its higher object variety and relatively sparse grasp annotation distribution given object geometry. For GraspSAM, the performance inversion may be attributed to its dependence on object masks, as these are obtained from ground truth in simulation for the Jacquard dataset but are predicted from RGB images for the Cornell dataset. We also notice that while query prompts help improve performance for LGD on the Cornell dataset by $\sim 5\%$, this does not have a noticeable effect on the Jacquard dataset. The closest method to our approach of language-driven, zero-shot transfer from large pretraining is LGD, which however performs poorly on both datasets. We attribute this to the limited coverage of expert grasp annotations as well as noisy ground truths on the GraspAnything++ dataset [15, 40].

B. Ablations

To demonstrate the operating principle of our design choices, we provide two sets of ablations for our approach. The first one analyzes the choice of VLM used by VLAD, in addition to examining the importance of the three-step prompting detailed in Sec. III-A. The second set of ablations deals with examining the effect of different pointcloud alignment methods for the cross-domain object alignment, comparing with our method for principal component-based correspondence-free optimization detailed in Sec. III-B.

Shown in Tab. II, GPT-5 performs the best in terms of generating a feasible grasp, with a success rate of 91.43%.

TABLE I: Success Rate (SR) for all methods on Cornell [11] and Jacquard [10] datasets. Following prior work [11], a grasp is deemed successful if its grasp rectangle has an Intersection over Union (IoU) of at least 25% with at least one of the ground truth annotations.

Method	Cornell	Jacquard
GR-ConvNet [34]	72.14 ± 41.19	59.62 ± 46.13
GG-CNN [33]	74.28 ± 40.30	71.48 ± 42.76
SE-ResUNet [35]	86.07 ± 28.65	88.14 ± 30.43
GraspSAM [16]	67.50 ± 44.19	73.71 ± 40.95
LGD w/ Query [15]	37.98 ± 44.81	24.40 ± 41.39
LGD w/o Query [15]	32.26 ± 42.47	24.40 ± 41.39
Ours (zero-shot)	91.43 ± 28.00	85.43 ± 36.15

Without the 3-Step prompting procedure, the success rate drops by more than 12%, although this comes with the trade-off of using $\sim 32\%$ fewer tokens as well as lower variance in grasp success. This aligns with our empirical observations that both the intermediate text-based reasoning R^g and the specificity of the generated query prompt T_2^g helps guide the image generation process to obtain a better goal image I_G and, consequently, a better object grasp. Gemini 2.5 [28] performs $\sim 7\%$ worse despite the higher number of reasoning tokens used, although with lower variance in grasp success. While the image portion of the output tokens is expected to be relatively similar across all approaches, the number of text output tokens is a useful metric for quantifying possibly more detailed intermediate reasoning R^g and the descriptiveness of the generated text query prompts T_2^g . We also explored utilizing a combination of Llama 4 [21] for text-based reasoning and StableDiffusion’s image-to-image model [44] for generating goal images. While the text outputs are reasonable, the generative model had extremely poor prompt adherence on the dataset images.

We present results for point cloud alignment approaches in Tab. III. In terms of grasp success rate, our approach (PCA+Opt + CfOpt) significantly outperforms the comparison methods – TEASER++ [45] by about 36% and Iterative Closest Point (ICP) [46] by about 57% – with a lower variance in grasp success rate. ICP performs the worst in terms of the Chamfer Distance (CD) and Unidirectional Hausdorff Distance (UHD), which we attribute to its myopic optimization routine which easily gets trapped in a local minima. Lastly, we notice that our method achieves $\sim 30\%$ lower CD but with a $\sim 30\%$ higher UHD, likely due to the choice of CD as the correspondence-free loss \mathcal{L} for optimization. This tradeoff reflects a key strength of our approach: Unlike methods that are sensitive to local feature alignment, our optimization prioritizes the global shape structure. This means that, for a case like ours where local features between o_S and o_G may differ or depth prediction errors distort finer details, the overall shape remains sufficiently similar across the cartesian spaces $\mathcal{C}_S, \mathcal{C}_G$ and are preserved to support downstream tasks.

C. Real World Deployment

We perform real-world evaluations of our method to demonstrate its feasibility for realistic tasks. We deploy our method on a Franka Research 3 robot with a Franka Panda Hand comprising a parallel jaw gripper. We obtain RGB-D observations with a wrist-mounted ORBBEC Femto Mega camera. The initial scene image I_S is captured from a top-

VLM	SR (%) \uparrow	# Tokens Used (10^3)	
		Output	Reasoning
GPT 5 [17]	91.43 ± 27.99	1.69 ± 1.01	2.11 ± 0.56
GPT 5 w/o 3-Step	78.57 ± 41.03	1.15 ± 0.52	0
Gemini 2.5 [18]	84.29 ± 36.39	1.73 ± 0.15	2.54 ± 1.15

TABLE II: Success Rate (SR), and number of output and reasoning tokens used for GPT 5 (with and without 3-Step prompting) and Gemini 2.5.

Method	SR (%) \uparrow	Alignment Metric \downarrow	
		CD (10^{-3})	UHD (10^{-2})
TEASER++ [45]	55.71 ± 49.67	0.24 ± 0.40	5.68 ± 3.91
ICP [46]	34.29 ± 47.47	76.8 ± 145.1	50.8 ± 68.8
PCA+Opt (Ours)	91.43 ± 27.99	0.17 ± 0.17	7.21 ± 6.48

TABLE III: Success Rate (SR), Chamfer Distance (CD), and Unidirectional Hausdorff Distance (UHD) for TEASER++, Iterative Closest Point (ICP), and principal component alignment followed by correspondence-free optimization (PCA+Opt; Ours).

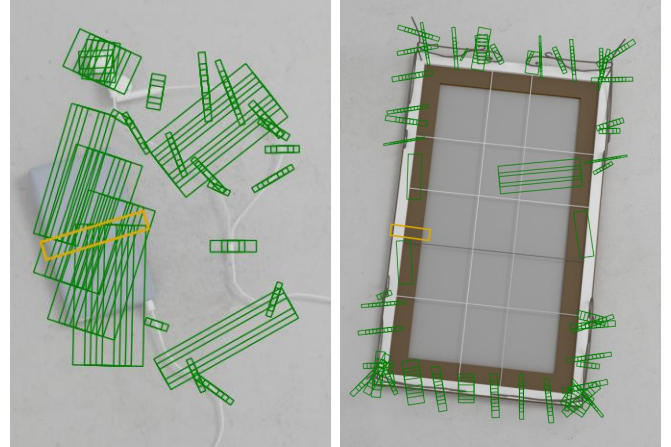


Fig. 4: Examples of viable grasps generated by our approach (yellow), improperly marked as failures due to high angular mismatch (left) and missing ground truth annotations near the predicted grasp (right).

down view, in accordance with the ideal dynamic range for the depth sensor, with a white background that mimics the setup of the Jacquard dataset. Following image capture, VLAD generates the optimal grasp location on the object and outputs an oriented grasp rectangle in the original image space I_S . The robot then uses its end-effector pose and the camera’s relative extrinsics to obtain an approximate grasp pose above the object. Next, the robot hand approaches the object, closes the gripper to grasp the object, and lifts for several seconds to validate a successful hold. If the object remains in the gripper when time elapses, we consider this a success, else failure. We present video demonstrations in the supplementary material, which show the robustness of our method’s performance in the real-world.

V. DISCUSSION

A. Dataset Coherence

The Cornell dataset comprises 885 real RGB-D images of objects taken from an angled top-down view with human-annotated grasps. The Jacquard dataset contains about 54k simulated images (RGB, perfect depth, and object masks) captured from a top-down view, along with automatically generated grasp annotations. Particularly, random grasp poses are sampled and annotated as success/failure based on a robot picking physics simulation. As the scale and object diversity of datasets increase, it naturally becomes more challenging to provide fully exhaustive grasp annotations for each data point, and both datasets suffer from this issue proportional

to their cardinality.

For both datasets, we observe that the distribution of ground-truth grasp annotations provided lacks full coverage of ground-truth grasp modes, given the object geometries. Grasp annotations for the Cornell dataset can sometimes miss viable grasp poses. However, this is mitigated by the lower object diversity and the use of human annotation for labeling ground-truth grasps. For the Jacquard dataset, while we are not privy to the sampling heuristic used, the annotations for successful grasps vary in quality, number, and distribution across the dataset. Naturally, this affects methods trained on these datasets by biasing them to the specific distribution of grasps seen in the training set, which upper-bounds their performance. Our method does not suffer from this issue, as it does not directly learn to grasp, but rather reasons about object geometry and properties to generate a grasp. Hence, our approach can generate valid grasps that are not represented in the evaluation dataset. However, some grasps generated by our method are incorrectly marked as failures, as indicated in Fig. 4. Our approach proposes grasping the music player (*left*) along the short axis; however, the grasp rectangle has an insufficient IoU with the ground-truth annotations to be marked as a success. For the canvas (*right*) with its back facing the camera, our approach proposes grasping it from the border of the frame; however, the absence of a corresponding ground-truth grasp in the dataset causes this valid proposal to be marked as a failure. We therefore argue that the performance indicated is a lower bound on the potential success rate in the wild.

B. Limitations

While the large-scale training of VLMs allows them to perform and generalize well for most generative tasks, this is not always reliable. In some cases, the VLM fails to accurately interpret the object in the input image, resulting in surreal or distorted structures that disrupt the global geometry of the original object. Such failures may arise from either imperfect object understanding or the intrinsic instability in the generation process. Similarly, prompt adherence is not guaranteed, and the VLM may generate content that deviates from the specified instructions, resulting in outputs that cannot be plausibly translated into actionable grasps. Secondly, the point cloud alignment module inherits imperfections from the depth prediction of generated images and segmentation. Inaccuracies in object masks or depth maps can compromise the quality of the point cloud generated for the object. This, in turn, can cause misalignment between the original and generated object point clouds, leading to incorrect grasp proposals. Although our alignment method is robust to local feature noise, errors in segmentation or depth can severely hinder the recovery of executable grasps. Finally, practical deployment is constrained by efficiency considerations. Querying large VLMs for image-conditioned generation is computationally expensive, and inference speeds are significantly slower than those of specialized grasp detection networks. This cost limits the immediate scalability of VLAD-Grasp to high-throughput or real-time applications. However, as the state

of research progresses, more feasible versions developed in the future can be plugged into our method, possibly achieving superior performance with better efficiency and throughout.

VI. CONCLUSION

We propose VLAD-Grasp, a zero-shot grasp synthesis framework that leverages the reasoning and generative capabilities of large-scale vision–language models. By formulating grasp detection as the generation of rod-impaled object images, and subsequently lifting this representation into 3D through depth prediction and geometric alignment, our approach bypasses the need for expert grasp annotations or retraining. Our training-free pipeline demonstrates that foundation models can serve as powerful priors for robotic manipulation.

Our experiments highlight several key strengths of VLAD-Grasp. First, the method achieves competitive or superior grasp success rates compared to state-of-the-art supervised models, despite no task-specific training. Second, the integration of structured prompting and geometric consistency ensures robust transfer from synthetic goal images to executable grasps in the real world. Finally, the successful deployment on a Franka Research 3 robot reinforces that the approach generalizes to novel, previously unseen objects, underscoring the generalizable reasoning capabilities of VLMs for robotic grasping.

ACKNOWLEDGMENTS

This material is based upon work supported in part by the DEVCOM Army Research Laboratory under cooperative agreement : W911NF2520170.

REFERENCES

- [1] M. Kulshrestha and A. H. Qureshi, “Structural concept learning via graph attention for multi-level rearrangement planning,” in *Conference on Robot Learning*. PMLR, 2023, pp. 3180–3193.
- [2] G. Zhai, X. Cai, D. Huang, Y. Di, F. Manhardt, F. Tombari, N. Navab, and B. Busam, “Sg-bot: Object rearrangement via coarse-to-fine robotic imagination on scene graphs,” in *2024 IEEE International Conference on Robotics and Automation (ICRA)*. IEEE, 2024, pp. 4303–4310.
- [3] M. Koskinopoulou, F. Raptopoulos, G. Papadopoulos, N. Mavrakis, and M. Maniadakis, “Robotic waste sorting technology: Toward a vision-based categorization system for the industrial robotic separation of recyclable waste,” *IEEE Robotics & Automation Magazine*, vol. 28, no. 2, pp. 50–60, 2021.
- [4] Z. Zhang, Y. Wang, Z. Zhang, L. Wang, H. Huang, and Q. Cao, “A residual reinforcement learning method for robotic assembly using visual and force information,” *Journal of Manufacturing Systems*, vol. 72, pp. 245–262, 2024.
- [5] A. K. Keshari, H. Ren, and A. H. Qureshi, “Cograsp: 6-dof grasp generation for human-robot collaboration,” in *2023 IEEE International Conference on Robotics and Automation (ICRA)*. IEEE, 2023, pp. 9829–9836.
- [6] L. Chen, G. Avula, H. Ren, Z. Wang, and A. H. Qureshi, “Multimodal human-intent modeling for contextual robot-to-human handovers of arbitrary objects,” *arXiv preprint arXiv:2508.02982*, 2025.
- [7] A. Bicchi and V. Kumar, “Robotic grasping and contact: A review,” in *Proceedings 2000 ICRA. Millennium conference. IEEE international conference on robotics and automation. Symposia proceedings (Cat. No. 00CH37065)*, vol. 1. IEEE, 2000, pp. 348–353.
- [8] R. M. Murray, Z. Li, and S. S. Sastry, *A mathematical introduction to robotic manipulation*. CRC press, 2017.
- [9] R. Newbury, M. Gu, L. Chumbley, A. Mousavian, C. Eppner, J. Leitner, J. Bohg, A. Morales, T. Asfour, D. Kragic *et al.*, “Deep learning

approaches to grasp synthesis: A review,” *IEEE Transactions on Robotics*, vol. 39, no. 5, pp. 3994–4015, 2023.

[10] A. Depierre, E. Dellandréa, and L. Chen, “Jacquard: A large scale dataset for robotic grasp detection,” in *2018 IEEE/RSJ International Conference on Intelligent Robots and Systems (IROS)*. IEEE, 2018, pp. 3511–3516.

[11] Y. Jiang, S. Mosen, and A. Saxena, “Efficient grasping from rgbd images: Learning using a new rectangle representation,” in *2011 IEEE International conference on robotics and automation*. IEEE, 2011, pp. 3304–3311.

[12] Q. Li and S. Yuan, “Jacquard v2: Refining datasets using the human in the loop data correction method,” in *2024 IEEE International Conference on Robotics and Automation (ICRA)*. IEEE, 2024, pp. 7932–7938.

[13] M. Shridhar, L. Manuelli, and D. Fox, “Cliport: What and where pathways for robotic manipulation,” in *Conference on robot learning*. PMLR, 2022, pp. 894–906.

[14] K. Xu, S. Zhao, Z. Zhou, Z. Li, H. Pi, Y. Zhu, Y. Wang, and R. Xiong, “A joint modeling of vision-language-action for target-oriented grasping in clutter,” *arXiv preprint arXiv:2302.12610*, 2023.

[15] A. D. Vuong, M. N. Vu, B. Huang, N. Nguyen, H. Le, T. Vo, and A. Nguyen, “Language-driven grasp detection,” in *Proceedings of the IEEE/CVF Conference on Computer Vision and Pattern Recognition*, 2024, pp. 17902–17912.

[16] S. Noh, J. Kim, D. Nam, S. Back, R. Kang, and K. Lee, “GraspSAM: When segment anything model meets grasp detection,” in *2025 IEEE International Conference on Robotics and Automation (ICRA)*. IEEE, 2025, pp. 14 023–14 029.

[17] A. Hurst, A. Lerer, A. P. Goucher, A. Perelman, A. Ramesh, A. Clark, A. Ostrow, A. Welihinda, A. Hayes, A. Radford *et al.*, “Gpt-4o system card,” *arXiv preprint arXiv:2410.21276*, 2024.

[18] G. Comanici, E. Bieber, M. Schaeckermann, I. Pasupat, N. Sachdeva, I. Dhillon, M. Blistein, O. Ram, D. Zhang, E. Rosen *et al.*, “Gemini 2.5: Pushing the frontier with advanced reasoning, multimodality, long context, and next generation agentic capabilities,” *arXiv preprint arXiv:2507.06261*, 2025.

[19] C. Team, “Chameleon: Mixed-modal early-fusion foundation models, 2024,” *URL https://arxiv. org/abs/2405.09818*, vol. 9, no. 8, 2024.

[20] J. Achiam, S. Adler, S. Agarwal, L. Ahmad, I. Akkaya, F. L. Aleman, D. Almeida, J. Alten Schmidt, S. Altman, S. Anadkat *et al.*, “Gpt-4 technical report,” *arXiv preprint arXiv:2303.08774*, 2023.

[21] H. Touvron, T. Lavril, G. Izacard, X. Martinet, M.-A. Lachaux, T. Lacroix, B. Rozière, N. Goyal, E. Hambro, F. Azhar *et al.*, “Llama: Open and efficient foundation language models,” *arXiv preprint arXiv:2302.13971*, 2023.

[22] Z. Li, X. Wu, H. Du, F. Liu, H. Nghiem, and G. Shi, “A survey of state of the art large vision language models: Benchmark evaluations and challenges,” in *Proceedings of the Computer Vision and Pattern Recognition Conference*, 2025, pp. 1587–1606.

[23] H. Hong, S. Wang, Z. Huang, Q. Wu, and J. Liu, “Why only text: empowering vision-and-language navigation with multi-modal prompts,” in *Proceedings of the Thirty-Third International Joint Conference on Artificial Intelligence*, 2024, pp. 839–847.

[24] A. Radford, J. W. Kim, C. Hallacy, A. Ramesh, G. Goh, S. Agarwal, G. Sastry, A. Askell, P. Mishkin, J. Clark *et al.*, “Learning transferable visual models from natural language supervision,” in *International conference on machine learning*. PMLR, 2021, pp. 8748–8763.

[25] J. Li, D. Li, C. Xiong, and S. Hoi, “Blip: Bootstrapping language-image pre-training for unified vision-language understanding and generation,” in *International conference on machine learning*. PMLR, 2022, pp. 12 888–12 900.

[26] J.-B. Alayrac, J. Donahue, P. Luc, A. Miech, I. Barr, Y. Hasson, K. Lenc, A. Mensch, K. Milligan, M. Reynolds *et al.*, “Flamingo: a visual language model for few-shot learning,” *Advances in neural information processing systems*, vol. 35, pp. 23 716–23 736, 2022.

[27] Z. Yang, L. Li, K. Lin, J. Wang, C.-C. Lin, Z. Liu, and L. Wang, “The dawn of lmms: Preliminary explorations with gpt-4v (ision),” *arXiv preprint arXiv:2309.17421*, 2023.

[28] G. Team, R. Anil, S. Borgeaud, J.-B. Alayrac, J. Yu, R. Soricut, J. Schalkwyk, A. M. Dai, A. Hauth, K. Milligan *et al.*, “Gemini: a family of highly capable multimodal models,” *arXiv preprint arXiv:2312.11805*, 2023.

[29] A. O’Neill, A. Rehman, A. Maddukuri, A. Gupta, A. Padalkar, A. Lee, A. Pooley, A. Gupta, A. Mandlekar, A. Jain *et al.*, “Open x-embodiment: Robotic learning datasets and rt-x models: Open x-embodiment collaboration 0,” in *2024 IEEE International Conference on Robotics and Automation (ICRA)*. IEEE, 2024, pp. 6892–6903.

[30] R. Firooz, J. Tucker, S. Tian, A. Majumdar, J. Sun, W. Liu, Y. Zhu, S. Song, A. Kapoor, K. Hausman *et al.*, “Foundation models in robotics: Applications, challenges, and the future,” *The International Journal of Robotics Research*, vol. 44, no. 5, pp. 701–739, 2025.

[31] I. Kapelyukh, V. Vosylius, and E. Johns, “Dall-e-bot: Introducing web-scale diffusion models to robotics,” *IEEE Robotics and Automation Letters*, vol. 8, no. 7, pp. 3956–3963, 2023.

[32] S. Karamcheti, S. Nair, A. S. Chen, T. Kollar, C. Finn, D. Sadigh, and P. Liang, “Language-driven representation learning for robotics,” *arXiv preprint arXiv:2302.12766*, 2023.

[33] D. Morrison, P. Corke, and J. Leitner, “Closing the loop for robotic grasping: A real-time, generative grasp synthesis approach,” *arXiv preprint arXiv:1804.05172*, 2018.

[34] S. Kumra, S. Joshi, and F. Sahin, “Antipodal robotic grasping using generative residual convolutional neural network,” in *2020 IEEE/RSJ International Conference on Intelligent Robots and Systems (IROS)*. IEEE, 2020, pp. 9626–9633.

[35] S. Ainetter and F. Fraundorfer, “End-to-end trainable deep neural network for robotic grasp detection and semantic segmentation from rgb,” in *2021 IEEE International Conference on Robotics and Automation (ICRA)*. IEEE, 2021, pp. 13 452–13 458.

[36] J. Mahler, J. Liang, S. Niyaz, M. Laskey, R. Doan, X. Liu, J. A. Ojea, and K. Goldberg, “Dex-net 2.0: Deep learning to plan robust grasps with synthetic point clouds and analytic grasp metrics,” *arXiv preprint arXiv:1703.09312*, 2017.

[37] A. Mousavian, C. Eppner, and D. Fox, “6-dof graspnet: Variational grasp generation for object manipulation,” in *Proceedings of the IEEE/CVF international conference on computer vision*, 2019, pp. 2901–2910.

[38] S. T. Bukhari, K. Agrawal, Z. Kingston, and A. Bera, “Variational shape inference for grasp diffusion on se (3),” *arXiv preprint arXiv:2508.17482*, 2025.

[39] C. Eppner, A. Mousavian, and D. Fox, “Acronym: A large-scale grasp dataset based on simulation,” in *2021 IEEE International Conference on Robotics and Automation (ICRA)*. IEEE, 2021, pp. 6222–6227.

[40] A. D. Vuong, M. N. Vu, H. Le, B. Huang, H. T. T. Binh, T. Vo, A. Kugi, and A. Nguyen, “Grasp-anything: Large-scale grasp dataset from foundation models,” in *2024 IEEE International Conference on Robotics and Automation (ICRA)*. IEEE, 2024, pp. 14 030–14 037.

[41] H. G. Barrow, J. M. Tenenbaum, R. C. Bolles, and H. C. Wolf, “Parametric correspondence and chamfer matching: Two new techniques for image matching,” *Tech. Rep.*, 1977.

[42] A. Bochkovskii, A. Delaunoy, H. Germain, M. Santos, Y. Zhou, S. R. Richter, and V. Koltun, “Depth pro: Sharp monocular metric depth in less than a second,” *arXiv preprint arXiv:2410.02073*, 2024.

[43] A. Kirillov, E. Mintun, N. Ravi, H. Mao, C. Rolland, L. Gustafson, T. Xiao, S. Whitehead, A. C. Berg, W.-Y. Lo *et al.*, “Segment anything,” in *Proceedings of the IEEE/CVF international conference on computer vision*, 2023, pp. 4015–4026.

[44] R. Rombach, A. Blattmann, D. Lorenz, P. Esser, and B. Ommer, “High-resolution image synthesis with latent diffusion models,” in *Proceedings of the IEEE/CVF conference on computer vision and pattern recognition*, 2022, pp. 10 684–10 695.

[45] H. Yang, J. Shi, and L. Carlone, “Teaser: Fast and certifiable point cloud registration,” *IEEE Transactions on Robotics*, vol. 37, no. 2, pp. 314–333, 2020.

[46] S. Rusinkiewicz and M. Levoy, “Efficient variants of the icp algorithm,” in *Proceedings third international conference on 3-D digital imaging and modeling*. IEEE, 2001, pp. 145–152.